

# Estimating the Ionospheric Induction Electric Field using Ground Magnetometers

Michael Madelaire<sup>1</sup>, Karl Laundal<sup>1</sup>, Spencer Hatch<sup>1</sup>, Heikki Vanhamäki<sup>2</sup>, Jone Reistad<sup>1</sup>, Anders Ohma<sup>1</sup>, Viacheslav Merkin<sup>3</sup>, and Dong Lin<sup>4</sup>

<sup>1</sup>Department of Physics and Technology, University of Bergen

<sup>2</sup>Space Physics and Astronomy Research Unit, University of Oulu

<sup>3</sup>Applied Physics Laboratory, Johns Hopkins University

<sup>4</sup>High Altitude Observatory, National Center for Atmospheric Research

April 16, 2024

## Abstract

The ionospheric convection electric field is often assumed to be a potential field. This assumption is not always valid, especially when the ionosphere changes on short time scales  $\sim 5$  min. We present a technique for estimating the induction electric field using ground magnetometer measurements. The technique is demonstrated on real and simulated data for sudden increases in solar wind dynamic pressure of  $\sim 1$  and 10 nPa, respectively. For the real data, the ionospheric induction electric field is  $0.15 \pm 0.015$  mV/m, and the corresponding compressional flow is  $2.5 \pm 0.3$  m/s. For the simulated data, the induction electric field and compressional flow reach 3 mV/m and 50 m/s, respectively. The induction electric field can locally constitute tens of percent of the total electric field. Inclusion of the induction electric field increased the total Joule heating by 2.4%. Locally the Joule heating changed by tens of percent. This corresponds to energy dissipation that is not accounted for in existing models.

# Estimating the Ionospheric Induction Electric Field using Ground Magnetometers

Michael Madelaire<sup>1</sup>, Karl Laundal<sup>1</sup>, Spencer Hatch<sup>1</sup>, Heikki Vanhamäki<sup>2</sup>, Jone Reistad<sup>1</sup>, Anders Ohma<sup>1</sup>, Viacheslav Merkin<sup>4</sup>, Dong Lin<sup>3</sup>

<sup>1</sup>Department of Physics and Technology, University of Bergen, Bergen, Norway

<sup>2</sup>Space Physics and Astronomy Research Unit, University of Oulu, Oulu, Finland

<sup>3</sup>High Altitude Observatory, National Center for Atmospheric Research, Boulder, CO, USA

<sup>4</sup>Applied Physics Laboratory, Johns Hopkins University, Laurel, MD, USA

## Key Points:

- A method for estimating the induction electric field using ground magnetometer measurements is presented.
- Locally, the induction electric field can constitute tens of percent of the total electric field, during the sudden commencement examined.
- The spatial pattern of ionospheric Joule heating is shown to be highly affected by the induction electric field, even during weak induction.

---

Corresponding author: Michael Madelaire, [michael.madelaire@uib.no](mailto:michael.madelaire@uib.no)

## Abstract

The ionospheric convection electric field is often assumed to be a potential field. This assumption is not always valid, especially when the ionosphere changes on short time scales  $T \lesssim 5$  min. We present a technique for estimating the induction electric field using ground magnetometer measurements. The technique is demonstrated on real and simulated data for sudden increases in solar wind dynamic pressure of  $\sim 1$  and 10 nPa, respectively. For the real data, the ionospheric induction electric field is  $0.15 \pm 0.015$  mV/m, and the corresponding compressional flow is  $2.5 \pm 0.3$  m/s. For the simulated data, the induction electric field and compressional flow reach 3 mV/m and 50 m/s, respectively. The induction electric field can locally constitute tens of percent of the total electric field. Inclusion of the induction electric field increased the total Joule heating by 2.4%. Locally the Joule heating changed by tens of percent. This corresponds to energy dissipation that is not accounted for in existing models.

## Plain Language Summary

In the study of ionospheric dynamics, it is often assumed that the ionospheric electric field is a potential field. This means the contribution from induction is neglected. The induction electric field is described by Faraday's law and relates to temporal changes in the magnetic field. This assumption only holds when the ionospheric dynamics change slowly. In this study, we present a technique for calculating the ionospheric induction electric field using measurements of the magnetic field on the ground. We demonstrate the technique on real and simulated data of a dynamic event, i.e. a sudden commencement. We find that the induction electric field, on a global scale, is small compared to the potential electric field. However, locally it can be relatively large. Similarly, the inclusion of the induction electric field increased the total energy dissipation, i.e. Joule heating, by only a couple of percent but resulted in local variations of tens of percent. Furthermore, we quantified and visualized the compression flow which is the compression and expansion of the magnetic field related to the temporal evolution of a dynamic ionospheric event.

## 1 Introduction

In this paper, we investigate the ionospheric induction electric field ( $\mathbf{E}_{ind}$ ) using a new technique based on ground magnetometers. When studying ionospheric dynamics the ionospheric electric field ( $\mathbf{E}$ ) is often assumed to be a potential field ( $\mathbf{E}_{pot}$ ). This assumption can be very useful as it may simplify modeling efforts significantly. Techniques such as AMIE/AMGeO [Richmond and Kamide 1988]; [AMGeO Collaboration 2019] and Lompe [Laundal et al. 2022]; [Hovland et al. 2022] model  $\mathbf{E}_{pot}$  by ignoring  $\mathbf{E}_{ind}$  that otherwise is implied by Faraday's induction law ( $\nabla \times \mathbf{E} = -\frac{\partial}{\partial t} \mathbf{B}$ ) [Faraday 1832]. Similarly,  $\mathbf{E}_{ind}$  is almost always ignored in the ionospheric solvers used to account for the magnetosphere-ionosphere (MI) coupling in magnetohydrodynamic (MHD) simulations (e.g. Tanaka 2000; J. Lyon et al. 2004; Merkin and J. G. Lyon 2010). We present a technique for estimating  $\mathbf{E}_{ind}$  based on measurements of ground magnetic perturbation. Essentially, allowing  $\mathbf{E}_{ind}$  to be measured from ground.

Transient events (e.g. sudden commencements or substorm expansions) can result in large changes in the magnetic field ( $\mathbf{B}$ ) on a timescale of seconds or minutes. When ignoring Faraday's law the mutual interaction between the electrostatic and inductive processes is neglected which can be important during dynamic events. Yoshikawa and Itonaga 2000 provide a detailed explanation of the inductive ionosphere, from an  $\mathbf{E}, \mathbf{J}$  perspective [Vasyliūnas 2012]. It is well known that field-aligned currents (FACs) close through the ionosphere via a divergent Pedersen current, assuming the ionospheric conductance is uniform and the system is in steady state. When a magnetospheric driver is changed, e.g. the opening of a magnetic field line and subsequent anti-sunward con-

66 vection, the information is communicated via shear Alfvén waves. Bending a magnetic  
 67 field line, in the conductive ionosphere, excites a flow of electrons perpendicular to the  
 68 direction of the bend (i.e. Ampere’s law) which constitutes a rotational electric field, i.e.  
 69  $\mathbf{E}_{ind}$ . Again, assuming uniform conductance, the flow of electrons is a divergent Hall cur-  
 70 rent. Because the electrons are *frozen-in* they act to compress/expand magnetic flux,  
 71 i.e.  $\frac{\partial}{\partial t}\mathbf{B}$ . We refer to this as *compression flow* ( $\mathbf{E}_{ind}\times\mathbf{B}$ ). The compression flow is nec-  
 72 essary to alter the distribution of magnetic flux to facilitate the ionospheric closure cur-  
 73 rent carried by ions and a new steady state. In other words, in steady state and uniform  
 74 conductance, the Pedersen current closing FACs only exist due to a pre-existing diver-  
 75 gent Hall current. The rate of change in the ionosphere depends on the Pedersen con-  
 76 ductance ( $\Sigma_P$ ). Southwood and Kivelson 1991 derived a decay rate ( $\gamma \propto \Sigma_P^{-1}$ ) describ-  
 77 ing the time it takes for the ionospheric current system to change. Additionally, Dreher  
 78 1997 simulated the MI coupling with inductive terms and showed that the time it takes  
 79 a FAC to reach steady state varies with  $\Sigma_P$ .

80 Vanhamäki et al. 2005 investigated the inductive effect on the ionospheric electric  
 81 field using realistic time-dependent three-dimensional models of the high latitude iono-  
 82 spheric current system. They found that ionospheric self-induction is locally important  
 83 with  $\mathbf{E}_{ind}$  reaching a few mV/m. Vanhamäki et al. 2006 presented a new technique for  
 84 calculating  $\mathbf{E}_{ind}$  in a non-uniform conducting ionosphere. The technique utilizes the Carte-  
 85 sian elementary current system technique and requires  $\mathbf{E}_{pot}$  and Hall/Pedersen conduc-  
 86 tances as input. Vanhamäki et al. 2007 applied this technique to derive  $\mathbf{E}_{ind}$  for a west-  
 87 ward traveling surge,  $\Omega$ -band, and intensifying electrojet. They found that  $\mathbf{E}_{ind}$  can reach  
 88 magnitudes of several tens of percent of the total electric field. Takeda 2008 simulated  
 89  $\mathbf{E}_{ind}$  associated with FACs with periods of 60, 10, 4, and 1 min and found that  $\mathbf{E}_{ind}$  had  
 90 a non-negligible impact when the period of the FACs was 4 min or less.

91 In this study, we present a technique for estimating the ionospheric induction elec-  
 92 tric field based on ground magnetometer measurements represented with a spherical har-  
 93 monic expansion and present examples of the associated ionospheric plasma flow. The  
 94 purpose of the presented technique is to go beyond the assumption of a potential elec-  
 95 tric field in empirical modeling (e.g., AMIE and Lompe). Co-estimation of the poten-  
 96 tial and induction electric fields is desirable to understand the temporal evolution of the  
 97 system. From a practical point of view, it also avoids the mapping of the induction elec-  
 98 tric field into the potential electric field. Additionally, by including the time-dependency  
 99 of the system, the result becomes more constrained as subsequent time-steps are linked  
 100 via measurements, increasing the overall information. However, the incorporation of this  
 101 technique into pre-existing empirical modeling frameworks is outside the scope of the cur-  
 102 rent study and will be addressed in future studies.

103 Our technique uses spatiotemporal variations in the magnetic field to infer com-  
 104 pressional flow is analogous with studies of core flow using time-dependent models of Earth’s  
 105 main magnetic field (e.g. Finlay et al. 2020; Sabaka et al. 2020; Finlay et al. 2023). Spher-  
 106 ical harmonic models of Earth’s core magnetic field can provide information about changes  
 107 in the motion of liquid metal in the outer core through estimates of secular variation.  
 108 This information can be used as boundary conditions in models of Earth’s dynamo [Scha-  
 109 effer et al. 2016]. To the knowledge of the authors, it is the first time ground magnetome-  
 110 ter measurements have been used to inform about the inductive component of the iono-  
 111 spheric electric field. However, Vanhamäki et al. 2013 solved Faraday’s law based on the  
 112 radial magnetic field to derive the induced electric field at Earth’s surface.

113 In Section 2 we present a technique for deriving the ionospheric  $\mathbf{E}_{ind}$  from ground  
 114 magnetic field perturbations. A more thorough derivation is provided in the Support-  
 115 ing Information. In Section 3, the technique is demonstrated using synthetic data from  
 116 a coupled geospace model presented by Shi et al. 2022 and real ground magnetometer  
 117 measurements during sudden commencements (SCs). Section 4 discusses the results.

## 2 Technique

In this section, we describe how an estimate of the ionospheric induction electric field ( $\mathbf{E}_{ind}$ ) can be derived from the temporal derivative of the radial magnetic field ( $\frac{\partial}{\partial t}B_r$ ) below the ionosphere. A more in-depth derivation is provided in the Supporting Information.

The ionospheric electric field ( $\mathbf{E}$ ) can be decomposed into three scalar fields using the *alternative Helmholtz representation* [Sabaka et al. 2010],

$$\mathbf{E} = U\hat{\mathbf{r}} + \nabla_S V - \hat{\mathbf{r}} \times \nabla_S W. \quad (1)$$

Here  $\hat{\mathbf{r}}$  is the radial unit vector and  $\nabla_S$  is the angular portion of the  $\nabla$  operator.

The curl of the ionospheric electric field ( $\nabla \times \mathbf{E}$ ) on a spherical shell can be described by  $\frac{\partial}{\partial t}B_r$  on the shell according to Faraday's law. By inserting Equation 1 into Faraday's law  $\frac{\partial}{\partial t}B_r$  can be expressed in terms of  $W$ ,

$$\frac{\partial}{\partial t}B_r = \hat{\mathbf{r}} \nabla^2 W. \quad (2)$$

The scalar field  $W$  can be represented with a Spherical Harmonic (SH) expansion,

$$W = \sum_{n=1}^N \sum_{m=0}^n [a_n^{m,W} \cos(m\phi) + b_n^{m,W} \sin(m\phi)] P_n^m(\cos(\theta)). \quad (3)$$

Here  $(\theta, \phi)$  are colatitude and longitude,  $(n, m)$  are the SH degree and order,  $(a_n^{m,W}, b_n^{m,W})$  are the SH coefficients, and  $P_n^m(\cos(\theta))$  is the Schmidt quasi normalized Legendre polynomial. The coefficients  $(a_n^{m,W}, b_n^{m,W})$  are unknown, but can be expressed in terms of the SH coefficients  $(\frac{\partial}{\partial t}a_n^{m,B}, \frac{\partial}{\partial t}b_n^{m,B})$  related to a SH expansion of  $\frac{\partial}{\partial t}B_r$  following Sabaka et al. 2010,

$$\begin{aligned} a_n^{m,W} &= \frac{r^2}{n+1} \frac{\partial}{\partial t} a_n^{m,B} \\ b_n^{m,W} &= \frac{r^2}{n+1} \frac{\partial}{\partial t} b_n^{m,B}. \end{aligned} \quad (4)$$

In practice  $a_n^{m,B}$  and  $b_n^{m,B}$  can be determined by solving a linear inverse problem with magnetic field measurements on ground as input. The resulting SH coefficients should be determined using the ionosphere as their reference height. However, if the coefficients are determined with Earth's surface as their reference height they can simply be upward continued to the ionosphere. This detail is important as it defines the altitude of the spherical shell on which  $\mathbf{E}_{ind}$  will be determined. Only the radial magnetic field component can be upward continued to the ionosphere because it is continuous across boundary layers, unlike the horizontal components.

The horizontal part of  $\mathbf{E}_{ind}$  is given by the last term of Equation 1,

$$\mathbf{E}_{ind,h} = -\hat{\mathbf{r}} \times \nabla_S W = -\hat{\mathbf{r}} \times \nabla W. \quad (5)$$

In the ionosphere, where the field-aligned conductivity is high, the electric field maps along the magnetic field making  $\mathbf{E} \cdot \mathbf{B} = 0$ . This allows for the determination of  $E_{ind,r}$ . However,  $\mathbf{E}_{pot}$  is typically unknown. By assuming radial magnetic field lines  $E_{ind,r} = -E_{pot,r}$  and the compression flow is given as

$$\mathbf{v} = \frac{\mathbf{E}_{ind} \times \hat{\mathbf{b}}_r}{B}, \quad (6)$$

where  $\hat{\mathbf{b}}_r = -\hat{\mathbf{r}}$  in the northern hemisphere.

Through the merger of the technique presented here and empirical modeling techniques of the ionospheric potential electric field like AMIE and Lompe  $\mathbf{E}_{pot}$  and  $\mathbf{E}_{ind}$  might be co-estimated. This will be the focus of future studies.

### 3 Results

Estimating the induction electric field ( $\mathbf{E}_{ind}$ ) requires a SH model of  $\frac{\partial}{\partial t} B_r$ . In this section, we apply our method to two different cases of SCs. One model is based on ground magnetic perturbations from an MHD simulation while the other is based on real ground magnetometer measurements.

#### 3.1 Synthetic data example

The synthetic data is based on an MHD simulation of an interplanetary shock carried out and analyzed by Shi et al. 2022. During this event, the solar wind dynamic pressure increases by approximately 10 nPa. The RE-developed Magnetosphere-Ionosphere Coupler/Solver (REMIX) [Merkin and J. G. Lyon 2010] is used to determine the ionospheric current and assumes that  $\nabla \times \mathbf{E} = 0$ . The reader is referred to Shi et al. 2022 for further details regarding the simulation. The ground magnetic perturbation is determined by computing a Biot-Savart integral over the ionospheric currents, FACs, and magnetospheric currents on an equal area grid with a 0.5 degree latitudinal resolution down to 0° latitude. We represent the ground magnetic perturbation using SHs, where the SH coefficients ( $a_n^{m,B}$ ,  $b_n^{m,B}$ ) are determined by solving an inverse problem similar to Madelaire et al. 2022a with the SH expansion truncated at  $n = 100$ . The SH expansion is only done for external sources as the synthetic data does not include ground induction.

Figure 1 summarizes the technique for estimating  $\mathbf{E}_{ind}$ , using synthetic data of the preliminary impulse associated with a SC. Figure 1a shows  $\frac{\partial}{\partial t} B_r$  on ground. Figure 1b shows a recreation of  $\frac{\partial}{\partial t} B_r$  using a SH model based on ground magnetic perturbation. A comparison between Figures 1a-b shows that  $\frac{\partial}{\partial t} B_r$  is reproduced well by the SH model. Figures 1c-d compare the estimated  $\mathbf{E}_{ind}$  and the ionospheric potential electric field ( $\mathbf{E}_{pot}$ ) from the MHD simulation. Comparison between  $\mathbf{E}_{ind}$  and  $\mathbf{E}_{pot}$  are done with respect to the first of the two subsequent timesteps used to determine  $\frac{\partial}{\partial t} B_r$ . We find that  $\mathbf{E}_{ind}$  reaches up to 3 mV/m which locally can correspond to tens of percent of  $\mathbf{E}$  ( $\mathbf{E} = \mathbf{E}_{pot} + \mathbf{E}_{ind}$ ) in the high latitude ionosphere. Therefore,  $\mathbf{E}_{ind}$  can have a significant regional impact. Figure 1e shows Joule heating associated with  $\mathbf{E}_{pot}$  (i.e.  $\Sigma_p E_{pot}^2$ ) which is a result of maintaining the steady state current system. Figure 1f shows the difference in Joule heating when including  $\mathbf{E}_{ind}$ , i.e.  $\Sigma_P [E_{pot}^2 + 2(\mathbf{E}_{pot} \cdot \mathbf{E}_{ind}) + E_{ind}^2]$ . The difference can locally be tens of percent, both positive and negative. However, the total Joule heating above 50 degrees latitude only increases by approximately 2.4%. The pins in Figures 1e-f illustrate the steady state convection and compression flow (Equation 6), respectively, where  $B$  is the magnitude of a dipole magnetic field. The dipole magnetic field is determined using the first SH degree of IGRF-12 [Thébault et al. 2015]. The flow illustrates the expansion/compression of magnetic flux necessary to change the ionospheric current system from one steady state to another.

#### 3.2 Real data example

The SH model based on real ground magnetometer measurements was provided by Madelaire et al. 2022a and is the product of a superposed epoch analysis of SCs. Madelaire et al. 2022a presented 12 models determined by dividing the list of SCs presented by Madelaire et al. 2022b into 12 groups based on the Interplanetary Magnetic Field (IMF) clock angle and dipole tilt angle. In this example, we use the model created for SCs during northward IMF and positive dipole tilt (Summer in the northern hemisphere). The model is based on 175 events, the majority of which experience solar wind dynamic pressure increases around 1–2 nPa. The much smaller pressure increases in this model compared to that used in Section 3.1 results in significantly smaller  $\frac{\partial}{\partial t} B_r$  and  $\mathbf{E}_{ind}$ . The SH model includes a separation between internal and external sources. Both sets of SH coefficients are upward continued to the ionosphere and combined before deriving  $\mathbf{E}_{ind}$ .

186 Furthermore, to assess uncertainty, 50 realizations of the model were created by resam-  
187 pling the events used as input.

188 Figure 2 shows a time series of  $\frac{\partial}{\partial t} B_r$  and compression flow associated with the SH  
189 model, based on real ground magnetometer measurements, starting 2 minutes prior to  
190 the initial increase in SYM-H [Iyemori et al. 2010]. Epochs are synonymous with min-  
191 utes. Here,  $\frac{\partial}{\partial t} B_r$  is the median across all 50 model realizations and the compression flow  
192 is the bias vector (e.g. Haaland et al. 2007) scaled with the median magnitude. The pre-  
193 liminary impulse appears in Figures 2a-b. The main impulse appears in Figure 2c, equa-  
194 torward and with the opposite polarity of the preliminary impulse. Over the following  
195 3 minutes (i.e. Figures 2d-f) the main impulse expands along the flanks toward the night-  
196 side while increasing in strength. The compression flow is around 2.5 m/s with a stan-  
197 dard deviation of around 0.3 m/s. Additionally, a large-scale southward flow appears shortly  
198 after the appearance of the preliminary impulse.

## 199 4 Discussion

200 We presented a technique for estimating the ionospheric induction electric field ( $\mathbf{E}_{ind}$ )  
201 using measurements of magnetic field perturbation below the ionosphere. The technique  
202 links a SH representation of the temporal derivative of the radial magnetic field ( $\frac{\partial}{\partial t} B_r$ )  
203 to a scalar field  $W$  representing  $\mathbf{E}_{ind}$ . In an example with synthetic data, we found that  
204  $\mathbf{E}_{ind}$  reaches values of 3 mV/m (Figure 1d) which locally can correspond to tens of per-  
205 cent of the combined ionospheric electric field ( $\mathbf{E} = \mathbf{E}_{pot} + \mathbf{E}_{ind}$ ) in the high latitude  
206 ionosphere. From estimates of  $\mathbf{E}_{ind}$  a compression flow of approximately 50 m/s was cal-  
207 culated (Figure 1b), which represents the necessary expansion/contraction of magnetic  
208 flux to reach a new steady state. The total Joule heating above 50 degrees latitude in-  
209 creased by approximately 2.4% while local changes were tens of percent (see Figures 1e-  
210 f). Inclusion of  $\mathbf{E}_{ind}$  in the calculation of Joule heating adds two terms, i.e.  $\Sigma_P E_{ind}^2$  and  
211  $2\Sigma_P(\mathbf{E}_{pot} \cdot \mathbf{E}_{ind})$ . Assuming  $E_{ind} = E_{pot}/10$  results in  $E_{ind}^2$  being 1% of  $E_{pot}^2$ . Mean-  
212 while, the cross-term can contribute up to 20% of the Joule heating depending on the  
213 alignment of  $\mathbf{E}_{ind}$  and  $\mathbf{E}_{pot}$ . However, the cross-term can be positive or negative. It is,  
214 therefore, unclear how much it contributes to the total heating when integrated over the  
215 entire ionosphere. The contribution from the cross-term is illustrated in Figure 1f and  
216 leads to a significant difference in ionospheric energy dissipation during dynamic events  
217 compared to the steady state case, even when  $E_{ind}$  is an order of magnitude smaller than  
218  $E_{pot}$ . However, the estimated value of 2.4% is specific for the synthetic case being stud-  
219 ied as both the magnitude and spatial extent of the temporally varying magnetic field  
220 depend on several exogenous parameters. Furthermore, the background level of Joule  
221 heating can also vary.

222 The MHD simulation carried out by Shi et al. 2022, used to create the synthetic  
223 data example in Section 3.1, applied the ionospheric solver REMIX [Merkin and J. G.  
224 Lyon 2010] which assumes steady state. Therefore, the ionospheric electric field is a po-  
225 tential electric field since ionospheric self-inductance is neglected (i.e.  $\nabla \times \mathbf{E} = \frac{\partial}{\partial t} \mathbf{B} =$   
226  $0$ ). We calculate  $\frac{\partial}{\partial t} \mathbf{B}$  as the difference between two steady states for demonstration pur-  
227 poses. The combined ionospheric electric field (i.e.  $\mathbf{E} = \mathbf{E}_{pot} + \mathbf{E}_{ind}$ ) no longer sat-  
228 isfy the current continuity ( $\nabla \cdot \mathbf{J} = 0$ ) ensured in REMIX and is fundamentally in-  
229 consistent. Furthermore, the rotational current associated with  $\mathbf{E}_{ind}$  in Figure 1d con-  
230 tributes to the ground magnetic perturbation. This leads to a secondary and weaker in-  
231 duction effect which subsequently leads to a third and so on and so forth. The infinite  
232 chain of opposing and progressively induction effects is naturally accounted for when us-  
233 ing real data. However, the synthetic data still provide insight into the usefulness of the  
234 presented technique. The magnitude of  $\mathbf{E}_{ind}$  is similar to previous studies [Vanhamäki  
235 et al. 2005]; [Vanhamäki et al. 2007].

236 The presented technique was also used on a SH model of SCs based on real ground  
 237 magnetometer measurements [Madelaire et al. 2022a]. The retrieved  $\mathbf{E}_{ind}$  and compression  
 238 flow is around  $0.15 \pm 0.015$  mV/m and  $2.5 \pm 0.3$  m/s (Figure 2), respectively. Addi-  
 239 tionally, the compression flow is dominated by a large-scale southward flow. This is con-  
 240 sistent with an intensification of the magnetic perturbation from magnetospheric sources  
 241 due to compression of the magnetosphere. The same intensification gives rise to a step-  
 242 like increase in SYM-H during SCs [Russell et al. 1994]; [Madelaire et al. 2022b]. A large-  
 243 scale flow is likewise present in the example with synthetic data, i.e. Figure 1f. In Fig-  
 244 ure 3 the contribution from magnetospheric currents to  $\mathbf{E}_{ind}$  (i.e. Figure 3b) and the as-  
 245 sociated Joule heating has been separated from that of ionospheric currents and FACs  
 246 (i.e. Figure 3c) for the synthetic example. Magnetospheric currents (e.g. magnetopause  
 247 and ring current) produce, to first order, a uniform magnetic field in  $\hat{\mathbf{z}}$ . At the poles, this  
 248 corresponds to a weakening of the magnetic field, an azimuthal induction electric field  
 249 (westward on the dayside), and a large-scale southward flow in the northern hemisphere.  
 250 The induction electric field in the southern hemisphere points in the same direction but  
 251  $\hat{\mathbf{b}}$  points outward giving rise to a large-scale northward compression flow. Essentially, there  
 252 is a large-scale equatorward compression flow at high latitude in response to rapid in-  
 253 creases in solar wind dynamic pressure. Oppositely, there is a large-scale poleward com-  
 254 pression flow in response to rapid decreases in solar wind dynamic pressure.

255 It is unclear how to interpret local changes in Joule heating due to the inclusion  
 256 of  $\mathbf{E}_{ind}$ . Hesse et al. 1997 showed that  $\mathbf{E}$  maps between the ionosphere and magneto-  
 257 sphere for ideal MHD, i.e. including inductive terms. If that holds in reality it would lead  
 258 to an asymmetric spatiotemporal evolution, e.g. during SCs. However, Hesse et al. 1997  
 259 also showed that the mapping is non-trivial in the presence of parallel electric fields. Re-  
 260 gardless of how  $\mathbf{E}_{ind}$  maps between ionosphere and magnetosphere the spatiotemporal  
 261 evolution of dynamic events, e.g. transient current vortices associated with the prelim-  
 262 inary and main impulse of a SC and rapid compression/expansion of the magnetosphere,  
 263 lead to significant local changes in Joule heating. The duration of these local changes  
 264 can result in ion upflow but are unlikely to cause neutral upwelling [Strangeway 2012].  
 265 Zou et al. 2017 observed lifting of the F region ionosphere, large and transient field-aligned  
 266 ion upflow, and prompt but short-lived ion temperature increase in the transition be-  
 267 tween the preliminary and main impulse of a sudden commencement using PFISR mea-  
 268 surements.

269 There are significant differences in the magnitude of  $\mathbf{E}_{ind}$  and the compression flow  
 270 (Equation 6) between the two models. The SH model provided by Madelaire et al. 2022a  
 271 is a product of a superposed epoch analysis based on a list of solar wind dynamic pres-  
 272 sure increases [Madelaire et al. 2022b]. The majority of the events in the list are not in-  
 273 terplanetary shocks, and experience smaller pressure increases compared to what is of-  
 274 ten seen in case studies and MHD simulations (e.g. Moretto et al. 2000; Slinker et al.  
 275 1999; Fujita et al. 2003. Madelaire et al. 2022b showed that the events, on average, con-  
 276 tain increases of a couple of nPa. The interplanetary shock simulated by Shi et al. 2022  
 277 increased by approximately 10 nPa. The vast difference in the size of the pressure in-  
 278 crease along with the smoothing associated with superposing multiple events leads to  
 279 a  $\frac{\partial}{\partial t} B_r$  in the order of 10 nT/min (Figure 2) compared to the 10 nT/s (Figure 1) seen  
 280 in the MHD simulation. This is likely the explanation for the smaller compression flow.

281 The presented technique can be extended to the Spherical Elementary Current Sys-  
 282 tem (SECS) technique [Amm and Viljanen 1999]. The Lompe technique [Laundal et al.  
 283 2022]; [Hovland et al. 2022] models  $\mathbf{E}_{pot}$  using SECS by combining various measurements  
 284 (e.g. conductance, convection, and ground/space magnetic field measurements), simi-  
 285 lar to AMIE/AMGeO [Richmond and Kamide 1988]; [AMGeO Collaboration 2019]. How-  
 286 ever, the use of SECS in Lompe makes it ideal for regional analysis. In the future, we  
 287 hope to remove the necessity of assuming steady state when using Lompe by implement-  
 288 ing a scheme to co-estimate  $\mathbf{E}_{pot}$  and  $\mathbf{E}_{ind}$  using a technique similar to the one shown

289 here. Looking ahead, preliminary work suggests that data from EISCAT 3D [Kero et al.  
 290 2019] will open possibilities for empirical modeling frameworks of 3D ionospheric cur-  
 291 rents. Such advancements will allow us to move beyond the limitations of an infinitely  
 292 thin ionosphere model. We might, therefore, revisit our technique in the future in attempts  
 293 to expand it into 3D.

## 294 Acknowledgments

295 This work was funded by the Research Council of Norway (RCN) under contract 223252/F50.  
 296 KL. and JR were also funded by the RCN under contract 300844/F50. KL. and SH were  
 297 also funded by the Trond Mohn Foundation. VM and DL were funded by NASA DRIVE  
 298 Science Center under cooperative Agreement 80NSSC22M0163.

## 299 Data Availability Statement

300 The synthetic data used in this study is available at Zenodo via [https://doi.org/](https://doi.org/10.5281/zenodo.8116401)  
 301 [10.5281/zenodo.8116401](https://doi.org/10.5281/zenodo.8116401) Madelaire 2023. The spherical harmonic model based on real  
 302 ground magnetometer observations was provided by Madelaire et al. 2022a and is avail-  
 303 able at Zenodo via <https://zenodo.org/record/6243103> Madelaire 2022.

## 304 References

- 305 AMGeO Collaboration (Dec. 2019). “A Collaborative Data Science Platform for the Geospace  
 306 Community: Assimilative Mapping of Geospace Observations (AMGeO) v1.0.0”. In:  
 307 *Zenodo*. DOI: [10.5281/zenodo.3564914](https://doi.org/10.5281/zenodo.3564914). URL: [https://doi.org/10.5281/](https://doi.org/10.5281/zenodo.3564914)  
 308 [zenodo.3564914](https://doi.org/10.5281/zenodo.3564914).
- 309 Amm, O. and A. Viljanen (June 1999). “Ionospheric disturbance magnetic field contin-  
 310 uation from the ground to the ionosphere using spherical elementary current sys-  
 311 tems”. In: *Earth, Planets and Space* 51.6, pp. 431–440. DOI: [10.1186/BF03352247](https://doi.org/10.1186/BF03352247).  
 312 URL: <https://doi.org/10.1186/BF03352247>.
- 313 Dreher, J. (1997). “On the self-consistent description of dynamic magnetosphere-ionosphere  
 314 coupling phenomena with resolved ionosphere”. In: *Journal of Geophysical Research:*  
 315 *Space Physics* 102.A1, pp. 85–94. DOI: <https://doi.org/10.1029/96JA02800>.  
 316 eprint: [https://agupubs.onlinelibrary.wiley.com/doi/pdf/10.1029/](https://agupubs.onlinelibrary.wiley.com/doi/pdf/10.1029/96JA02800)  
 317 [96JA02800](https://agupubs.onlinelibrary.wiley.com/doi/pdf/10.1029/96JA02800). URL: [https://agupubs.onlinelibrary.wiley.com/doi/abs/10.](https://agupubs.onlinelibrary.wiley.com/doi/abs/10.1029/96JA02800)  
 318 [1029/96JA02800](https://agupubs.onlinelibrary.wiley.com/doi/abs/10.1029/96JA02800).
- 319 Faraday, M. (1832). “V. Experimental researches in electricity”. In: *Philosophical Trans-*  
 320 *actions of the Royal Society of London* 122, pp. 125–162. DOI: [10.1098/rstl.1832.](https://doi.org/10.1098/rstl.1832.0006)  
 321 [0006](https://doi.org/10.1098/rstl.1832.0006). eprint: [https://royalsocietypublishing.org/doi/pdf/10.1098/rstl.](https://royalsocietypublishing.org/doi/pdf/10.1098/rstl.1832.0006)  
 322 [1832.0006](https://royalsocietypublishing.org/doi/pdf/10.1098/rstl.1832.0006). URL: [https://royalsocietypublishing.org/doi/abs/10.1098/](https://royalsocietypublishing.org/doi/abs/10.1098/rstl.1832.0006)  
 323 [rstl.1832.0006](https://royalsocietypublishing.org/doi/abs/10.1098/rstl.1832.0006).
- 324 Finlay, C. C., N. Gillet, J. Aubert, P. W. Livermore, and D. Jault (June 2023). “Gyres,  
 325 jets and waves in the Earth’s core”. In: *Nature Reviews Earth & Environment* 4.6,  
 326 pp. 377–392. DOI: [10.1038/s43017-023-00425-w](https://doi.org/10.1038/s43017-023-00425-w). URL: [https://doi.org/10.](https://doi.org/10.1038/s43017-023-00425-w)  
 327 [1038/s43017-023-00425-w](https://doi.org/10.1038/s43017-023-00425-w).
- 328 Finlay, C. C., C. Kloss, N. Olsen, M. D. Hammer, L. Tøffner-Clausen, A. Grayver, and  
 329 A. Kuvshinov (2020). “The CHAOS-7 geomagnetic field model and observed changes  
 330 in the South Atlantic Anomaly”. In: *Earth Planets Space* 72.156. DOI: [https://](https://doi.org/10.1186/s40623-020-01252-9)  
 331 [doi.org/10.1186/s40623-020-01252-9](https://doi.org/10.1186/s40623-020-01252-9).

- 332 Fujita, S., T. Tanaka, T. Kikuchi, K. Fujimoto, K. Hosokawa, and M. Itonaga (2003).  
 333 “A numerical simulation of the geomagnetic sudden commencement: 1. Generation  
 334 of the field-aligned current associated with the preliminary impulse”. In: *Journal*  
 335 *of Geophysical Research: Space Physics* 108.A12. DOI: [https://doi.org/10.](https://doi.org/10.1029/2002JA009407)  
 336 [1029/2002JA009407](https://doi.org/10.1029/2002JA009407).
- 337 Haaland, S. E., G. Paschmann, M. Förster, J. M. Quinn, R. B. Torbert, C. E. McIlwain,  
 338 H. Vaith, P. A. Puhl-Quinn, and C. A. Kletzing (2007). “High-latitude plasma con-  
 339 vection from Cluster EDI measurements: method and IMF-dependence”. In: *An-*  
 340 *nales Geophysicae* 25.1, pp. 239–253. DOI: [10.5194/angeo-25-239-2007](https://doi.org/10.5194/angeo-25-239-2007). URL:  
 341 <https://angeo.copernicus.org/articles/25/239/2007/>.
- 342 Hesse, Michael, Joachim Birn, and Robert A. Hoffman (1997). “On the mapping of iono-  
 343 spheric convection into the magnetosphere”. In: *Journal of Geophysical Research:*  
 344 *Space Physics* 102.A5, pp. 9543–9551. DOI: <https://doi.org/10.1029/96JA03999>.  
 345 eprint: [https://agupubs.onlinelibrary.wiley.com/doi/pdf/10.1029/](https://agupubs.onlinelibrary.wiley.com/doi/pdf/10.1029/96JA03999)  
 346 [96JA03999](https://agupubs.onlinelibrary.wiley.com/doi/pdf/10.1029/96JA03999). URL: [https://agupubs.onlinelibrary.wiley.com/doi/abs/10.](https://agupubs.onlinelibrary.wiley.com/doi/abs/10.1029/96JA03999)  
 347 [1029/96JA03999](https://agupubs.onlinelibrary.wiley.com/doi/abs/10.1029/96JA03999).
- 348 Hovland, A. Ø., K. M. Laundal, J. P. Reistad, S. M. Hatch, S. J. Walker, M. Madelaire,  
 349 and A. Ohma (2022). “The Lompe code: A Python toolbox for ionospheric data anal-  
 350 ysis”. In: *Frontiers in Astronomy and Space Sciences* 9. DOI: [10.3389/fspas.2022.](https://doi.org/10.3389/fspas.2022.1025823)  
 351 [1025823](https://doi.org/10.3389/fspas.2022.1025823). URL: [https://www.frontiersin.org/articles/10.3389/fspas.](https://www.frontiersin.org/articles/10.3389/fspas.2022.1025823)  
 352 [2022.1025823](https://www.frontiersin.org/articles/10.3389/fspas.2022.1025823).
- 353 Iyemori, T., M. Takeda, M. Nose, and H. Toh (2010). “Mid-latitude Geomagnetic Indices  
 354 ASY and SYM for 2009 (Provisional)”. In: *Internal Report of Data Analysis Cen-*  
 355 *ter for Geomagnetism and Space Magnetism, Kyoto University, Japan*.
- 356 Kero, J., D. Kastinen, J. Vierinen, T. Grydeland, C. Heinselman, J. Markkanen, and A.  
 357 Tjulin (2019). “EISCAT 3D: the next generation international atmosphere and geospace  
 358 research radar”. In: *Proceedings of the First NEO and Debris Detection Conference*.
- 359 Laundal, K. M., J. P. Reistad, S. M. Hatch, M. Madelaire, S. Walker, A. Hovland, A.  
 360 Ohma, V. Merkin, and K. Sorathia (May 2022). “Local Mapping of Polar Ionospheric  
 361 Electrodynamics”. In: *Journal of Geophysical Research: Space Physics* 127. DOI: [10.](https://doi.org/10.1029/2022JA030356)  
 362 [1029/2022JA030356](https://doi.org/10.1029/2022JA030356).
- 363 Lyon, J.G., J.A. Fedder, and C.M. Mobarry (2004). “The Lyon–Fedder–Mobarry (LFM)  
 364 global MHD magnetospheric simulation code”. In: *Journal of Atmospheric and Solar-*  
 365 *Terrestrial Physics* 66.15. Towards an Integrated Model of the Space Weather Sys-  
 366 tem, pp. 1333–1350. DOI: <https://doi.org/10.1016/j.jastp.2004.03.020>.  
 367 URL: <https://www.sciencedirect.com/science/article/pii/S1364682604001439>.
- 368 Madelaire, M. (Feb. 2022). *List of rapid solar wind dynamic pressure increases*. Zenodo  
 369 [Dataset]. DOI: [10.5281/zenodo.6243103](https://doi.org/10.5281/zenodo.6243103). URL: [https://doi.org/10.5281/](https://doi.org/10.5281/zenodo.6243103)  
 370 [zenodo.6243103](https://doi.org/10.5281/zenodo.6243103).
- 371 — (May 2023). *Synthetic data for estimation of the ionospheric induction electric field*.  
 372 Zenodo. [Dataset]. DOI: [10.5281/zenodo.8116401](https://doi.org/10.5281/zenodo.8116401). URL: [https://doi.org/10.](https://doi.org/10.5281/zenodo.8116401)  
 373 [5281/zenodo.8116401](https://doi.org/10.5281/zenodo.8116401).
- 374 Madelaire, M., K. M. Laundal, J. P. Reistad, S. M. Hatch, and A. Ohma (2022a). “Tran-  
 375 sient high latitude geomagnetic response to rapid increases in solar wind dynamic  
 376 pressure”. In: *Frontiers in Astronomy and Space Sciences* 9. DOI: [10.3389/fspas.](https://doi.org/10.3389/fspas.2022.953954)  
 377 [2022.953954](https://doi.org/10.3389/fspas.2022.953954). URL: [https://www.frontiersin.org/articles/10.3389/](https://www.frontiersin.org/articles/10.3389/fspas.2022.953954)  
 378 [fspas.2022.953954](https://www.frontiersin.org/articles/10.3389/fspas.2022.953954).

- 379 Madelaire, M., K. M. Laundal, J. P. Reistad, S. M. Hatch, A. Ohma, and S. Haaland  
 380 (2022b). “Geomagnetic Response to Rapid Increases in Solar Wind Dynamic Pres-  
 381 sure: Event Detection and Large Scale Response”. In: *Frontiers in Astronomy and*  
 382 *Space Sciences* 9. DOI: 10.3389/fspas.2022.904620. URL: [https://www.frontiersin.](https://www.frontiersin.org/article/10.3389/fspas.2022.904620)  
 383 [org/article/10.3389/fspas.2022.904620](https://www.frontiersin.org/article/10.3389/fspas.2022.904620).
- 384 Merkin, V. G. and J. G. Lyon (2010). “Effects of the low-latitude ionospheric boundary  
 385 condition on the global magnetosphere”. In: *Journal of Geophysical Research: Space*  
 386 *Physics* 115.A10. DOI: <https://doi.org/10.1029/2010JA015461>. eprint: [https://](https://agupubs.onlinelibrary.wiley.com/doi/pdf/10.1029/2010JA015461)  
 387 [agupubs.onlinelibrary.wiley.com/doi/pdf/10.1029/2010JA015461](https://agupubs.onlinelibrary.wiley.com/doi/pdf/10.1029/2010JA015461).  
 388 URL: [https://agupubs.onlinelibrary.wiley.com/doi/abs/10.1029/](https://agupubs.onlinelibrary.wiley.com/doi/abs/10.1029/2010JA015461)  
 389 [2010JA015461](https://agupubs.onlinelibrary.wiley.com/doi/abs/10.1029/2010JA015461).
- 390 Moretto, T., A. J. Ridley, M. J. Engebretson, and O. Rasmussen (2000). “High-latitude  
 391 ionospheric response to a sudden impulse event during northward IMF conditions”.  
 392 In: *Journal of Geophysical Research: Space Physics* 105.A2, pp. 2521–2531. DOI: <https://doi.org/10.1029/1999JA900475>.  
 393 [//doi.org/10.1029/1999JA900475](https://doi.org/10.1029/1999JA900475).
- 394 Richmond, A. D. and Y. Kamide (1988). “Mapping electrodynamic features of the high-  
 395 latitude ionosphere from localized observations: Technique”. In: *Journal of Geophys-*  
 396 *ical Research* 93.A6, pp. 5741–5759. DOI: 10.1029/JA093iA06p05741. URL: <https://doi.org/10.1029/JA093iA06p05741>.  
 397 [//doi.org/10.1029/JA093iA06p05741](https://doi.org/10.1029/JA093iA06p05741).
- 398 Russell, C. T., M. Ginskey, and S. M. Petrinec (Jan. 1994). “Sudden impulses at low-  
 399 latitude stations: Steady state response for northward interplanetary magnetic field”.  
 400 In: *Journal of Geophysical Research: Space Physics* 99.A1, pp. 253–261. DOI: <https://doi.org/10.1029/93JA02288>.  
 401 [//doi.org/10.1029/93JA02288](https://doi.org/10.1029/93JA02288).
- 402 Sabaka, T. J., G. Hulot, and N. Olsen (2010). “Mathematical Properties Relevant to Ge-  
 403 omagnetic Field Modeling”. English. In: *Handbook of Geomathematics*. Springer. DOI:  
 404 10.1007/978-3-642-27793-1\_17-2.
- 405 Sabaka, T. J., L. Tøffner-Clausen, N. Olsen, and C. C. Finlay (June 2020). “CM6: a com-  
 406 prehensive geomagnetic field model derived from both CHAMP and Swarm satel-  
 407 lite observations”. In: *Earth, Planets and Space* 72.1, p. 80. DOI: 10.1186/s40623-  
 408 020-01210-5. URL: <https://doi.org/10.1186/s40623-020-01210-5>.
- 409 Schaeffer, N., E. Silva, and M. A. Pais (June 2016). “Can Core Flows inferred from Ge-  
 410 omagnetic Field Models explain the Earth’s Dynamo?” In: *Geophysical Journal In-*  
 411 *ternational* 204. DOI: 10.6084/m9.figshare.1439333.
- 412 Shi, Xueling et al. (2022). “Geospace Concussion: Global Reversal of Ionospheric Ver-  
 413 tical Plasma Drift in Response to a Sudden Commencement”. In: *Geophysical Re-*  
 414 *search Letters* 49.19. e2022GL100014 2022GL100014, e2022GL100014. DOI: <https://doi.org/10.1029/2022GL100014>. eprint: [https://agupubs.onlinelibrary.](https://agupubs.onlinelibrary.wiley.com/doi/pdf/10.1029/2022GL100014)  
 415 [wiley.com/doi/pdf/10.1029/2022GL100014](https://agupubs.onlinelibrary.wiley.com/doi/pdf/10.1029/2022GL100014). URL: [https://agupubs.onlinelibrary.](https://agupubs.onlinelibrary.wiley.com/doi/abs/10.1029/2022GL100014)  
 416 [wiley.com/doi/abs/10.1029/2022GL100014](https://agupubs.onlinelibrary.wiley.com/doi/abs/10.1029/2022GL100014).  
 417 [wiley.com/doi/abs/10.1029/2022GL100014](https://agupubs.onlinelibrary.wiley.com/doi/abs/10.1029/2022GL100014).
- 418 Slinker, S. P., J. A. Fedder, W. J. Hughes, and J. G. Lyon (1999). “Response of the iono-  
 419 sphere to a density pulse in the solar wind: Simulation of traveling convection vor-  
 420 tices”. In: *Geophysical Research Letters* 26.23, pp. 3549–3552. DOI: [https://doi.](https://doi.org/10.1029/1999GL010688)  
 421 [org/10.1029/1999GL010688](https://doi.org/10.1029/1999GL010688).
- 422 Southwood, D. J. and M. G. Kivelson (1991). “An approximate description of field-aligned  
 423 currents in a planetary magnetic field”. In: *Journal of Geophysical Research: Space*  
 424 *Physics* 96.A1, pp. 67–75. DOI: <https://doi.org/10.1029/90JA01806>. eprint:  
 425 <https://agupubs.onlinelibrary.wiley.com/doi/pdf/10.1029/90JA01806>.

- 426 URL: [https://agupubs.onlinelibrary.wiley.com/doi/abs/10.1029/](https://agupubs.onlinelibrary.wiley.com/doi/abs/10.1029/90JA01806)  
427 [90JA01806](https://agupubs.onlinelibrary.wiley.com/doi/abs/10.1029/90JA01806).
- 428 Strangeway, R. J. (2012). “The equivalence of Joule dissipation and frictional heating  
429 in the collisional ionosphere”. In: *Journal of Geophysical Research: Space Physics*  
430 117.A2. DOI: <https://doi.org/10.1029/2011JA017302>. eprint: [https://](https://agupubs.onlinelibrary.wiley.com/doi/pdf/10.1029/2011JA017302)  
431 [agupubs.onlinelibrary.wiley.com/doi/pdf/10.1029/2011JA017302](https://agupubs.onlinelibrary.wiley.com/doi/pdf/10.1029/2011JA017302). URL:  
432 <https://agupubs.onlinelibrary.wiley.com/doi/abs/10.1029/2011JA017302>.
- 433 Takeda, Masahiko (2008). “Effects of the induction electric field on ionospheric current  
434 systems driven by field-aligned currents of magnetospheric origin”. In: *Journal of*  
435 *Geophysical Research: Space Physics* 113.A1. DOI: [https://doi.org/10.1029/](https://doi.org/10.1029/2007JA012662)  
436 [2007JA012662](https://doi.org/10.1029/2007JA012662). eprint: [https://agupubs.onlinelibrary.wiley.com/doi/pdf/](https://agupubs.onlinelibrary.wiley.com/doi/pdf/10.1029/2007JA012662)  
437 [10.1029/2007JA012662](https://agupubs.onlinelibrary.wiley.com/doi/pdf/10.1029/2007JA012662). URL: [https://agupubs.onlinelibrary.wiley.com/](https://agupubs.onlinelibrary.wiley.com/doi/abs/10.1029/2007JA012662)  
438 [doi/abs/10.1029/2007JA012662](https://agupubs.onlinelibrary.wiley.com/doi/abs/10.1029/2007JA012662).
- 439 Tanaka, T. (2000). “The state transition model of the substorm onset”. In: *Journal of*  
440 *Geophysical Research: Space Physics* 105.A9, pp. 21081–21096. DOI: [https://doi.](https://doi.org/10.1029/2000JA900061)  
441 [org/10.1029/2000JA900061](https://doi.org/10.1029/2000JA900061). eprint: [https://agupubs.onlinelibrary.wiley.](https://agupubs.onlinelibrary.wiley.com/doi/pdf/10.1029/2000JA900061)  
442 [com/doi/pdf/10.1029/2000JA900061](https://agupubs.onlinelibrary.wiley.com/doi/pdf/10.1029/2000JA900061). URL: [https://agupubs.onlinelibrary.](https://agupubs.onlinelibrary.wiley.com/doi/abs/10.1029/2000JA900061)  
443 [wiley.com/doi/abs/10.1029/2000JA900061](https://agupubs.onlinelibrary.wiley.com/doi/abs/10.1029/2000JA900061).
- 444 Thébault, E. et al. (May 2015). “International Geomagnetic Reference Field: the 12th  
445 generation”. In: *Earth, Planets and Space* 67.1, p. 79. DOI: 10.1186/s40623-015-  
446 0228-9. URL: <https://doi.org/10.1186/s40623-015-0228-9>.
- 447 Vanhamäki, H., O. Amm, and A. Viljanen (2006). “New method for solving inductive  
448 electric fields in the non-uniformly conducting ionosphere”. In: *Annales Geophys-*  
449 *icae* 24.10, pp. 2573–2582. DOI: 10.5194/angeo-24-2573-2006. URL: [https:](https://angeo.copernicus.org/articles/24/2573/2006/)  
450 [//angeo.copernicus.org/articles/24/2573/2006/](https://angeo.copernicus.org/articles/24/2573/2006/).
- 451 — (2007). “Role of inductive electric fields and currents in dynamical ionospheric sit-  
452 uations”. In: *Annales Geophysicae* 25.2, pp. 437–455. DOI: 10.5194/angeo-25-  
453 437-2007. URL: <https://angeo.copernicus.org/articles/25/437/2007/>.
- 454 Vanhamäki, H., A. Viljanen, and O. Amm (2005). “Induction effects on ionospheric elec-  
455 tric and magnetic fields”. In: *Annales Geophysicae* 23.5, pp. 1735–1746. DOI: 10.  
456 5194/angeo-23-1735-2005. URL: [https://angeo.copernicus.org/articles/](https://angeo.copernicus.org/articles/23/1735/2005/)  
457 [23/1735/2005/](https://angeo.copernicus.org/articles/23/1735/2005/).
- 458 Vanhamäki, H., A. Viljanen, R. Pirjola, and O. Amm (Sept. 2013). “Deriving the geo-  
459 magnetically induced electric field at the Earth’s surface from the time derivative  
460 of the vertical magnetic field”. In: *Earth, Planets and Space* 65.9, pp. 997–1006. DOI:  
461 10.5047/eps.2013.03.013. URL: [https://doi.org/10.5047/eps.2013.03.](https://doi.org/10.5047/eps.2013.03.013)  
462 [013](https://doi.org/10.5047/eps.2013.03.013).
- 463 Vasyliūnas, V M (Feb. 2012). “The physical basis of ionospheric electrodynamics”. In:  
464 *Ann. Geophys.* 30.2, pp. 357–369. DOI: 10.5194/angeo-30-357-2012. URL: [https:](https://www.ann-geophys.net/30/357/2012/%20https://www.ann-geophys.net/30/357/2012/angeo-30-357-2012.pdf)  
465 [//www.ann-geophys.net/30/357/2012/%20https://www.ann-geophys.net/](https://www.ann-geophys.net/30/357/2012/%20https://www.ann-geophys.net/30/357/2012/angeo-30-357-2012.pdf)  
466 [30/357/2012/angeo-30-357-2012.pdf](https://www.ann-geophys.net/30/357/2012/angeo-30-357-2012.pdf).
- 467 Yoshikawa, A. and M. Itonaga (2000). “The nature of reflection and mode conversion  
468 of MHD waves in the inductive ionosphere: Multistep mode conversion between di-  
469 vergent and rotational electric fields”. In: *Journal of Geophysical Research: Space*  
470 *Physics* 105.A5, pp. 10565–10584. DOI: <https://doi.org/10.1029/1999JA000159>.  
471 eprint: [https://agupubs.onlinelibrary.wiley.com/doi/pdf/10.1029/](https://agupubs.onlinelibrary.wiley.com/doi/pdf/10.1029/1999JA000159)

472 1999JA000159. URL: [https://agupubs.onlinelibrary.wiley.com/doi/abs/](https://agupubs.onlinelibrary.wiley.com/doi/abs/10.1029/1999JA000159)  
473 [10.1029/1999JA000159](https://agupubs.onlinelibrary.wiley.com/doi/abs/10.1029/1999JA000159).

474 Zou, S., D. Ozturk, R. Varney, and A. Reimer (2017). “Effects of sudden commencement  
475 on the ionosphere: PFISR observations and global MHD simulation”. In: *Geophys-*  
476 *ical Research Letters* 44.7, pp. 3047–3058. DOI: [https://doi.org/10.1002/](https://doi.org/10.1002/2017GL072678)  
477 [2017GL072678](https://doi.org/10.1002/2017GL072678). eprint: [https://agupubs.onlinelibrary.wiley.com/doi/pdf/](https://agupubs.onlinelibrary.wiley.com/doi/pdf/10.1002/2017GL072678)  
478 [10.1002/2017GL072678](https://agupubs.onlinelibrary.wiley.com/doi/pdf/10.1002/2017GL072678). URL: [https://agupubs.onlinelibrary.wiley.com/](https://agupubs.onlinelibrary.wiley.com/doi/abs/10.1002/2017GL072678)  
479 [doi/abs/10.1002/2017GL072678](https://agupubs.onlinelibrary.wiley.com/doi/abs/10.1002/2017GL072678).

2011-10-24 18:30:30 to 18:30:50

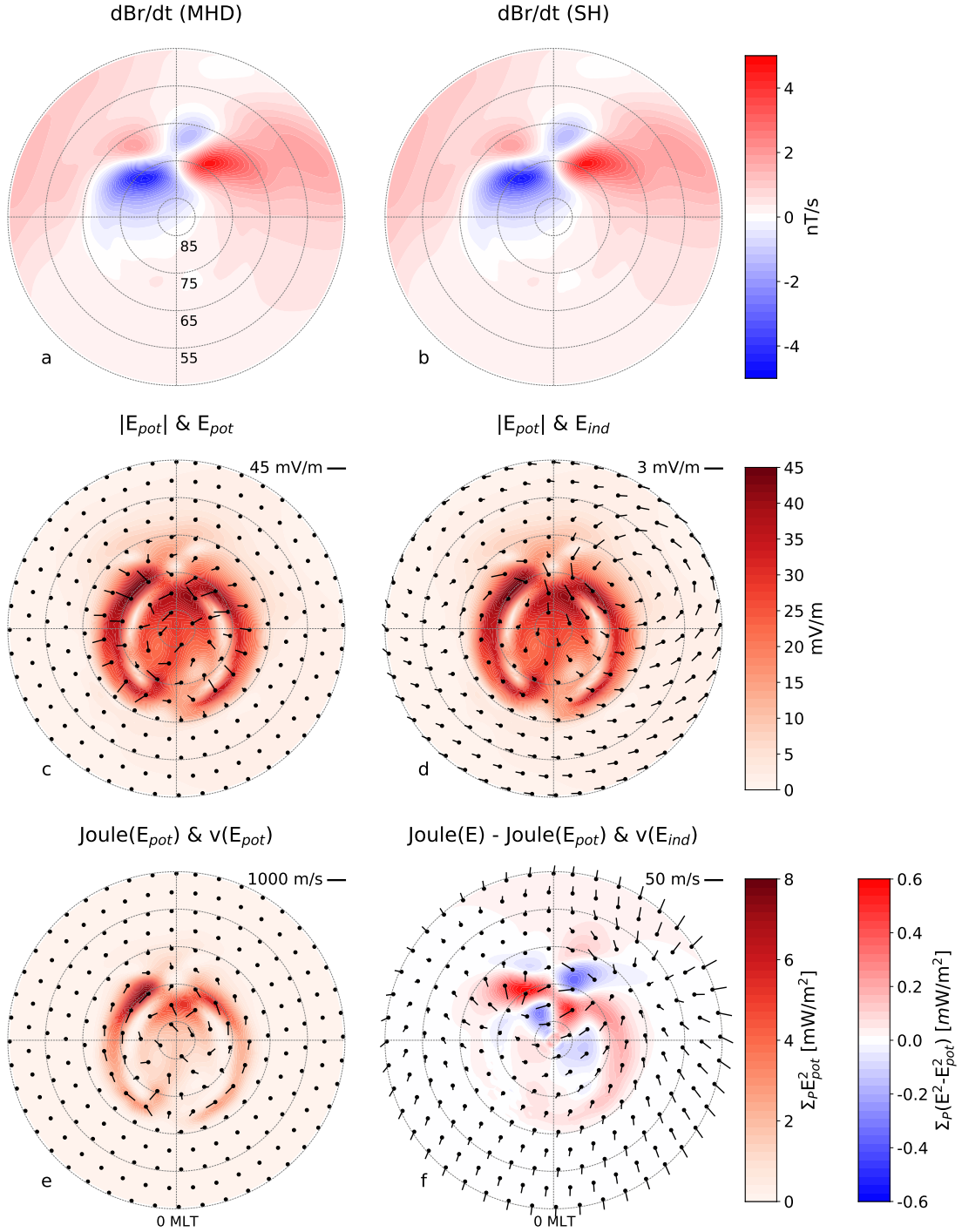


**Figure 1.** A summary of how  $\mathbf{E}_{ind}$  is determined based on synthetic ground magnetometer measurements from an MHD simulation [Shi et al. 2022], along with the compression flow and Joule heating. Figures 1a-b show  $\frac{\partial}{\partial t} B_r$  from the MHD and SH model, respectively. Figure 1c shows the magnitude of  $\mathbf{E}_{pot}$  and its orientation as pins. Figure 1d shows the magnitude of  $\mathbf{E}_{pot}$  with the orientation of  $\mathbf{E}_{ind}$  overlain. Figure 1e shows the Joule heating and plasma convection associated with  $\mathbf{E}_{pot}$  as a contour and pins, respectively. Figure 1f shows the difference between Joule heating associated with  $\mathbf{E}_{pot}$  and  $\mathbf{E} = \mathbf{E}_{pot} + \mathbf{E}_{ind}$  as well as the compression flow associated with  $\mathbf{E}_{ind}$ . The purpose of this figure is to validate the SH models' recreation of  $\frac{\partial}{\partial t} B_r$  as well as demonstrate the technique for estimating  $\mathcal{E}_{ind}$ .

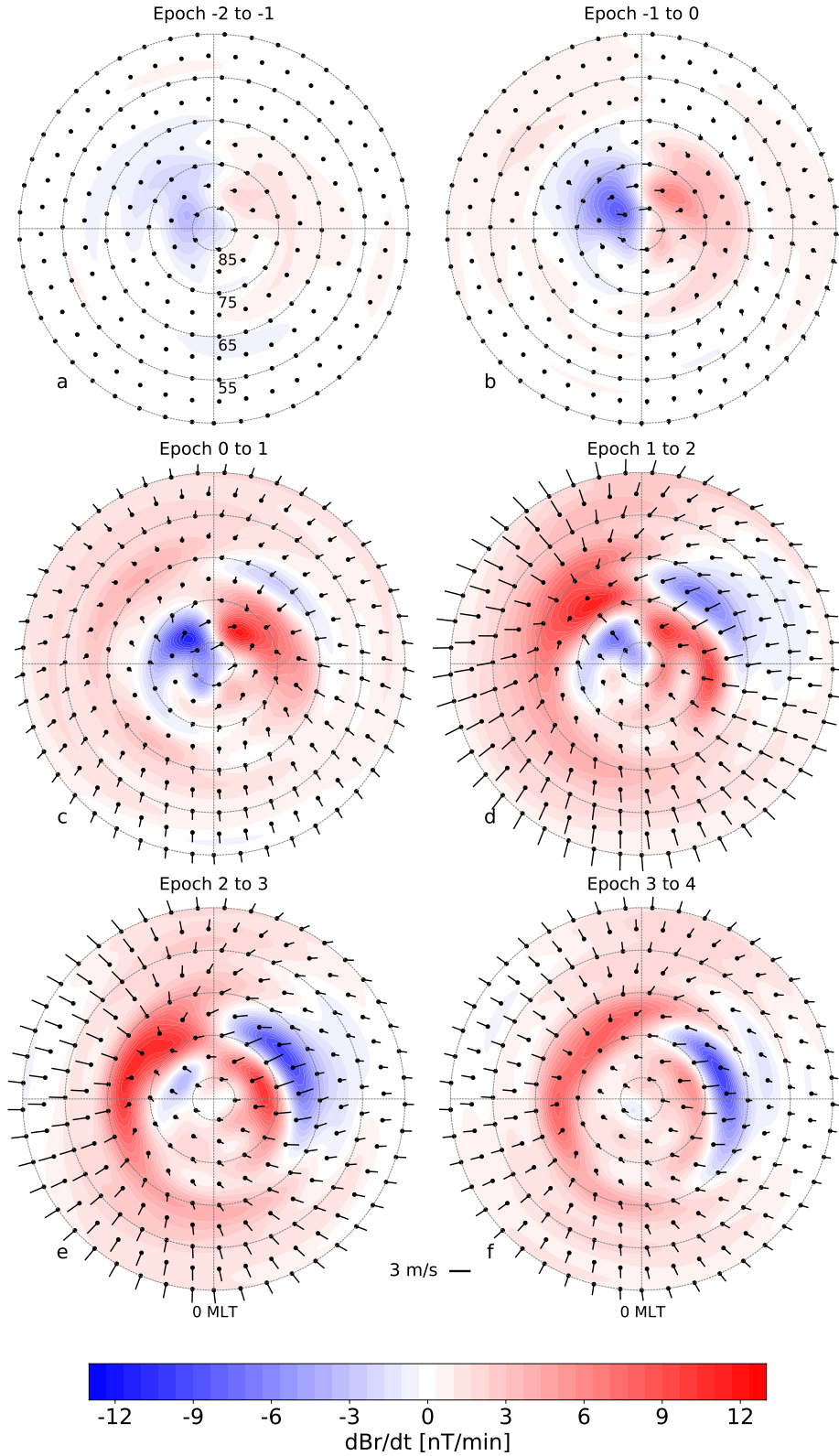


**Figure 2.** Illustration of  $\frac{\partial}{\partial t}B$  and  $\mathbf{E}_{ind} \times \mathbf{B}_0$  drift based on the SH model provided by Madeleine et al. 2022b. Epoch is synonymous with minute. The purpose of this figure is to showcase the estimation of  $\mathbf{E}_{ind}$  using a SH model that is based on real ground magnetometer measurements. Furthermore, the data includes contributions from magnetospheric sources that give rise to a large-scale southward compression flow.

2011-10-24 18:30:30 to 18:30:50

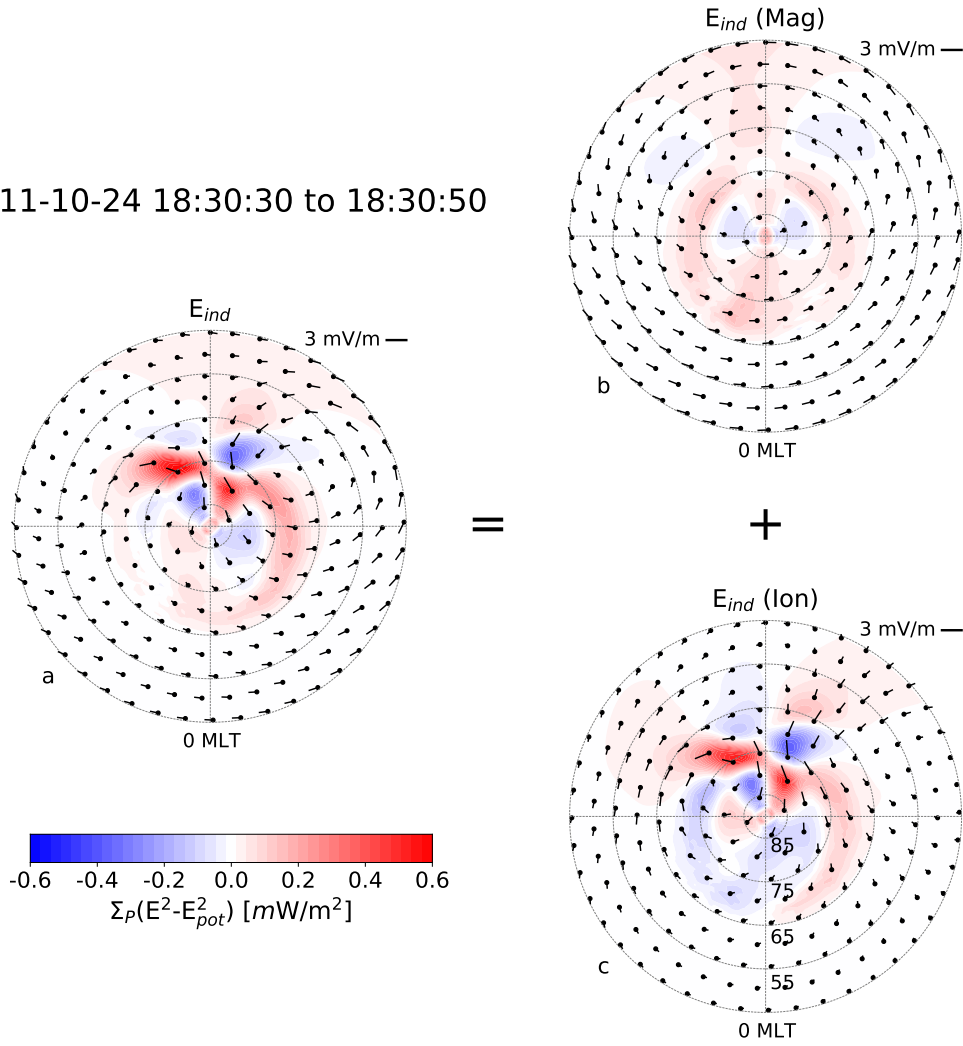


**Figure 3.** A decomposition of the contribution to  $\mathbf{E}_{ind}$  and associated Joule heating. Figure 3a shows the modification to the Joule heating when including  $\mathbf{E}_{ind}$  as a contour similar to Figure 1f with  $\mathbf{E}_{ind}$  superposed as pins. Figure 3b shows the contribution from magnetospheric currents while Figure 3c shows the contribution from ionospheric currents and FACs.